# High density Monte Carlo simulations of chain molecules: Bulk equation of state and density profile near walls

Ronald Dickman

*Department of Physics and Astronomy, Herbert H. Lehman College, CUNY, Bronx, New York 10468*

Carol K. Hall

*Department of Chemical Engineering, North Carolina State University, Raleigh, North Carolina 27695-7905*

We introduce a new Monte Carlo method suitable for simulations of chain molecules over a wide range of densities. Results for the equation of state of chains composed of 4, 8, and 16 freely joined hard spheres are compared with the predictions of several theories. The density profile of the fluid in the vicinity of the wall, and the scaling of the pressure with chain length are also discussed.

## I. INTRODUCTION

The statics and dynamics of fluids composed of chain molecules are topics of continuing interest, for basic theoretical as well as technological reasons.[1-3] Despite this interest, it is only recently that progress has been made toward developing accurate equations of state for simple model fluids (e.g., hard-sphere chains) in continuous space,[4-7] and there is also a paucity of simulation data for such models. In view of the central role that the theory of the hard-sphere system has played in understanding *monatomic* fluids,[8] it is natural to expect that a clear understanding of the hard-sphere chain fluid will spur progress in the study of more realistic models of polymeric fluids. In this paper we present a new method for determining the equation of state from simulations of model chain-molecule fluids, and compare our results with the predictions of several theories.

In a recent paper (Ref. 6, referred to as I in the following), we pointed out the discrepancy between the Flory lattice equation of state[9] and the behavior of chains in continuous space. We proposed that instead of directly applying the formula derived for the lattice model, the mean-field approach should be generalized by adopting, in a continuous-space context, the probabilistic assumptions invoked in Flory's theory. The resulting predictions for the equation of state compared quite favorably with the results of our Monte Carlo simulations of hard-sphere and hard-disk chains. However, the simulation method (test-chain insertion) employed in I did not permit investigation of the very interesting high-density regime, and was not well suited to the study of longer chains. In this paper we introduce a new simulation method, applicable over the full range of fluid densities, in which the pressure is found from the density of chain segments in contact with the wall. (The relation between pressure and hard-wall contact density has been known for a long time[10] in the case of monatomic fluids, but has not, to our knowledge, been employed previously for determining the equation of state.) We describe the method in Sec. II. In Sec. III we present our results for fluids composed of chains of 4, 8, and 16 freely jointed hard spheres, and compare them with the predictions of several theories.

## II. MONTE CARLO METHOD

In our previous simulations of chain molecules (I) the pressure was derived from the probability of nonoverlapping insertion of a "test chain" into an existing configuration. As the volume fraction $\eta = \rho\pi\sigma^3/6$ ($\sigma$ is the hard-sphere diameter) is increased, the insertion probability decays rapidly, and cannot be accurately estimated in simulations. In studies of chains composed of four tangent hard spheres, the test-chain insertion method was found to be almost useless beyond $\eta = 0.24$. (For comparison, note that the hard sphere system freezes at $\eta = 0.497$.) In simulations of *monatomic* fluids, the pressure may be computed from the radial distribution function $g(r)$. However, this method is not useful for molecular fluids with rigidly fixed bond lengths, since the pressure formula involves intermolecular correlation functions which depend on relative orientation as well as distance.[11] Calculation of the pressure via this method would require numerical estimation of three-body distributions. The method described below is much more direct, and provides information about the structure of the fluid in the vicinity of a wall. (Simulation in the constant-pressure ensemble[12,13] is an alternative method for determining the equation of state without computing correlation functions. It has yet to be applied to chain-molecule fluids.)

Consider a monatomic fluid in the presence of a hard wall, i.e., the potential

$$V(x) = \begin{cases} +\infty, & x < 0 \\ 0, & x > 0 \end{cases} \tag{2.1}$$

and let $\rho(x)$ denote the particle density at a distance $x$ from the wall. As was noted by Percus,[10] the particles are effectively decoupled at the wall, and revert to ideal-gas behavior:

$$\rho(0) = p/k_B T \equiv \pi^* \tag{2.2}$$

regardless of the intermolecular potential. Our Monte Carlo method is based on a straightfoward extension of this observation to a fluid composed of chain molecules.

In our studies the simulation cell has hard walls at $x = 0$ and $x = H$. In the other directions we impose periodic

boundary conditions with length $L$. The configurational partition function for a system of $N_p$ $n$-mers in such a cell is

$$Z(N, L, H) = (N_p!)^{-1} \int dx_1^{(1)} \cdots dx_{N_p}^{(n)} e^{-\beta U}$$

$$\times \prod_{i,j} \theta(x_i^{(j)})\theta(H - x_i^{(j)}), \qquad (2.3)$$

where $x_i^{(j)}$ is the position of the $j$th segment on the $i$th chain, and $\theta(x)$ is the heaviside step function. $U(\{x_i\})$ is the potential energy (including interactions between images in different periodic cells in the $y$ and $z$ directions). $U$ also includes the intersegment potentials which define the chain structure. For an isotropic fluid the pressure may be expressed in the form

$$\pi^* = \frac{1}{L^2} \frac{\partial}{\partial H} \log Z(N, L, H)$$

$$= (L^2 Z)^{-1} \int dx_1^{(1)} \cdots dx_{N_p}^{(n)} e^{-\beta U}$$

$$\times \prod_{i,j} \theta(x_i^{(j)})\theta(H - x_i^{(j)}) \sum_{ij} \delta(x_i^{(j)} - H)$$

$$= \rho(0), \qquad (2.4)$$

where

$$\rho(x) = N_p (L^2 Z)^{-1} \sum_{l=1}^{n} \int dx_2^{(1)} \cdots dx_{N_p}^{(n)}$$

$$\times \prod_{i,j} \theta(x_i^{(j)})\theta(H - x_i^{(j)}) \int_{x_1^{(l)} = x} dx_1^{(l)} e^{-\beta U} \qquad (2.5)$$

is the segment density at a distance $x$ from the wall and $\delta(x)$ is the Dirac delta function. The relation between pressure and hard-wall contact density, Eq. (2.4), holds for general interactions within and among molecules, since the potential energy $U$ is not affected by the $H$ derivative. An alternative route to Eq. (2.4) parallels Henderson and van Swol's derivation[14] of Eq. (2.2), in which the condition of local hydrostatic equilibrium in an external potential is integrated from the wall into the bulk fluid [see Eqs. (2)–(6) of Ref. 14]. It is trivial to extend this argument to a molecular fluid, if the chain molecule structure is incorporated into the intersegment potential $U$.

It is important to note that while the fluid is anisotropic in the vicinity of the wall, $\rho(0)$ represents the *bulk* pressure (i.e., the volume derivative of the free energy), which is a *scalar* quantity if the fluid is isotropic *in bulk*. In simulations employing the hard-wall contact density for determination of the pressure, it is important to check that the bulk fluid is isotropic. If the simulation cell is too small, orientation effects imposed by the walls may propagate into the central region, particularly at densities close to the freezing transition. As will be shown below, the present study is free of significant anisotropy or finite-size induced errors.

In this work we consider monodisperse systems of flexible chains, composed of tangent hard spheres. The separation between centers of successive segments is fixed at unit distance (one sphere diameter). Since the only interaction between segments is hard-sphere volume exclusion, the Boltzmann factor $e^{-\beta U}$, for a given arrangement is either

zero or unity. The temperature dependence is then trivial, and the model is said to be "athermal."

It has been noted[15-17] that the equilibrium properties of this model depend on whether one imposes the fixed bond-length constraint before or after performing the momentum integrations in the partition function. Applying the constraints prior to momentum integration corresponds to the usual canonical ensemble. This ensemble is the natural approach for describing the athermal model fluid under molecular dynamics simulations, since it provides a proper account of the constraints affecting the momenta. (Note that upon integration of the momenta, this ensemble yields a *nonuniform* configuration space density.) The ensemble pertinent to our simulations (and to the theories against which we compare our results!), is *not* the canonical ensemble, but rather an ensemble in which the *configuration space* probability density is proportional to $e^{-\beta U}$. In the present instance of athermal chains, the configuration space density is uniform on the subspace of allowed (i.e., $U = 0$) configurations. In this ensemble, which evidently corresponds to the usual Monte Carlo sampling procedure, momenta are not considered. In effect, the momenta have been integrated over, *prior* to imposition of the fixed bondlength constraint. The connection between canonical and "Monte Carlo" ensembles can be made through the so-called "metric determinant."[15]

Our configuration-space sampling procedure is as follows: Trial configurations are generated by (1) subjecting a randomly chosen chain "$i$" to a random uniform displacement: $x_i^{(j)} \rightarrow x_i^{(j)} + a$ ($j = 1,...,n$), and (2) subjecting the bond vectors $e_i^{(j)} = x_i^{(j+1)} - x_i^{(j)}$ ($j = 1,...,n - 1$) along the chain to independent random displacements, subject to the constraint $|e_i^{(j)}| = 1$. (This is accomplished by adding a random vector $b_j$ to $e_i^{(j)}$ and normalizing the resultant to unit length.) In a straightforward application of the Metropolis algorithm,[18] trial configurations are accepted if and only if they are free of overlap, both internally and with the walls. The average magnitudes of the random vectors $a$ and $b_j$ are adjusted to achieve an acceptance rate of about 30%. To estimate $\rho(x)$, we divide the cell into slabs of thickness $\Delta$ and compute the average segment density in each slab. This furnishes estimates for $\rho(x)$ at $x = \Delta/2, 3\Delta/2$, etc., from which the contact density is extrapolated.

Initial configurations are prepared by inserting, without overlap, randomly generated chains into the simulation cell. In this manner one may attain volume fractions $\eta \lesssim 0.28$. To reach higher densities, it is necessary to compress the system. This is accomplished by moving the walls inward, so that they are always in contact with the extreme segments, i.e., $H = \max_{ij} x_i^{(j)} - \min_{ij} x_i^{(j)}$, and $dH/dt < 0$. In some instances compression was hastened by imposing anisotropic displacement probabilities, driving the chains toward the midplane of the cell. (The length $L$ of the cell in the $y$ and $z$ directions was fixed at 10 in simulations of 4- and 8-mers, and at 12 in simulations of 16-mers.)

Initial configurations generated by chain insertion typically required a relaxation period of about $10^6$ trials for the density profile to attain a steady value. Relaxation periods of from $2 \times 10^6$ to $6 \times 10^6$ trials were necessary for initial condi-

tions prepared by compression. The final configuration of a run was often used to generate the initial configuration for a run at another density, attained by compression or expansion. In such instances relaxation periods of at least $10^6$ trials were again required. Criteria used to determine whether the system had relaxed were: (1) agreement between $\rho(x)$ values near the upper and lower walls, (2) overall symmetry of the density profile about $x = H/2$; and (3) steady values of the pressure in successive runs at the same density (i.e., with the final configuration of one run serving as the initial configuration for the next). The last mentioned is the most stringent condition, with (1) and (2) serving to rule out patently nonequilibrium configurations.

Our estimates of the density profile are based upon a series of at least ten runs, each consisting of at least $10^5$ trial moves. At higher densities, and for longer chains, longer simulations were needed, extending to a maximum of $10^7$ (total) trial moves, in large-cell simulations at the highest densities. The simulations with $H \leqslant 16$ were performed on a microVAX-2; the CPU time per step was approximately $1.5 \times 10^{-5} n^2 N_p$ s. The large-cell simulations ($H \geqslant 20$) were performed on mainframes, with a CPU time of approximately $5 \times 10^{-7} n^2 N_p$ s per step.

In interpreting the simulation results it is essential that the nonuniform distribution of segments be accounted for. Since the simulations are intended to model a macroscopic fluid which is *uniform away from the wall*, the physically relevant density is the bulk value $\rho_b$ (or the corresponding bulk volume fraction, $\eta_b = \frac{1}{6}\rho_b \pi \sigma^3$), in the central region of the cell, rather than the average density. (Of course, if the density profile shows significant variations in the central portion of the cell, one cannot expect the simulation to reflect bulk fluid behavior.) The bulk density was computed by averaging the density over the central region, i.e., the region over which the density profile does not exhibit systematic variation. This region typically comprised the inner 60% of the cell, but in the high density studies with $H \leqslant 10$, the bulk density was estimated from a more restricted region.

## III. SIMULATION RESULTS

We have performed Monte Carlo simulations of fluids composed of chains of 4, 8, and 16 tangent hard spheres, using the method described in the preceding section. We begin our presentation of results with a discussion of the segment-density profile. The density profile $\rho(x)$ of a hard-sphere (monatomic) fluid, in the presence of a hard wall, has been found, in theoretical studies,[10,19-21] and in simulations,[14,22] to exhibit an oscillatory structure, qualitatively similar to that of the radial distribution function, $g(r)$. At high densities there is a sharp peak at $x = 0$, and a series of progressively smaller and more diffuse peaks at $x = \sigma$, $2\sigma$, etc. The structure of the hard sphere fluid at a hard wall may be understood as resulting from an effective "field of mean force" (entropic in origin), which packs particles against the wall. At high densities the structure of the hard-sphere chain fluid is similar to that of the monatomic fluid, and we again expect $\rho(x)$ to be sharply peaked at the wall. But in the

chain-molecule fluid there is a compensating tendency toward depletion of the region near the wall, due to the reduction in configurational entropy of chains located there. The latter effect assumes greater importance at low densities, and for longer chains.

The density profiles observed in our simulations reflect the competing tendencies noted above. A sharp maximum at contact, and a pronounced oscillatory structure are evident at moderate and high densities, as in Figs. 1–3 (for $n = 4$) and Fig. 4 ($n = 8$). [These are plots of $n(x)$, the segment-density normalized to its bulk value.] At the highest densities there is a suggestion of a cusp-like singularity at $x = \sigma$. The cusp in $n(x)$ is a consequence of the fixed nearest-neighbor distance between chain segments in our model. (The radial distribution function of the rigid dimer fluid is known to exhibit such cusps.[23,24]) The tendency toward depletion of the region near the wall is dominant for longer chains and at low densities. Thus in Fig. 1 (open circles: $n = 4$, $\eta_b = 0.107$), and in Fig. 4 (open circles: $n = 16$, $\eta_b = 0.148$), $n(x)$ is depressed at the wall.

As noted above, the pressure is found by extrapolating $n(x)$ to its contact value. The typical behavior of the density profile near the wall is shown in Fig. 5, which illustrates the case $n = 4$, $\eta_b = 0.417$. In the vicinity of the wall, $\rho(x)$ values fall close to a straight line. The uncertainty in the estimate for the contact value is based on the statistical uncertainty in the data points near the wall, and on the spread of the points about the extrapolated straight line.

The simulation results for the compressibility factor $\rho_n^{-1} \pi^*$ ($\rho_n$ is the bulk $n$-mer density) are presented in Tables I–III, for $n = 4$, 8, and 16, respectively. These data, and several theoretical predictions for the compressibility factor, are plotted vs volume fraction in Figs. 6–8. In Fig. 6 (for $n = 4$) the results of our earlier simulations (I), which used the test chain insertion method, are also plotted. The agreement between the two methods rules out significant errors due to the influence of the walls, at least for $\eta < 0.25$. At
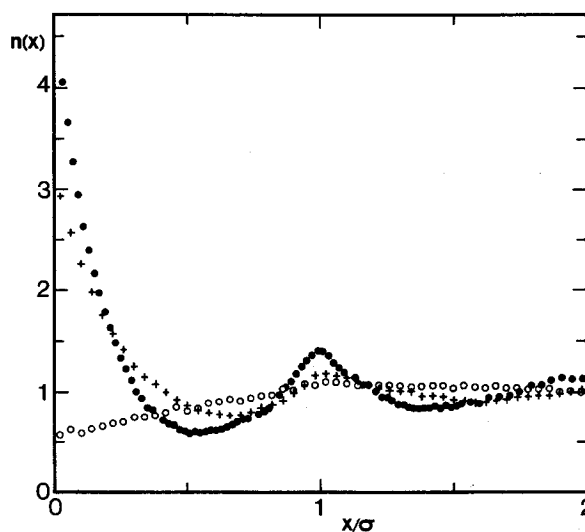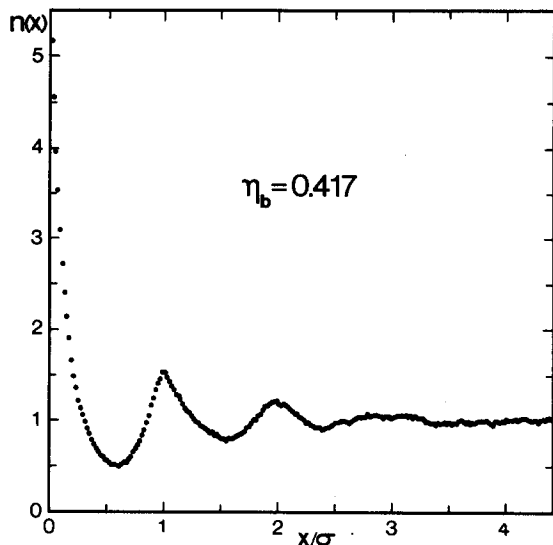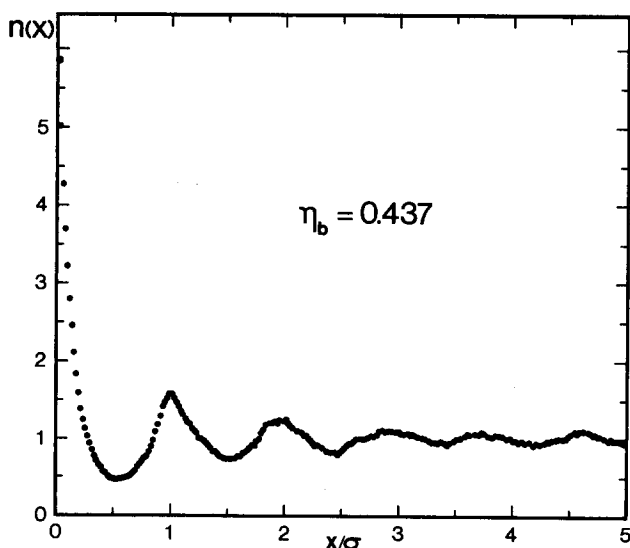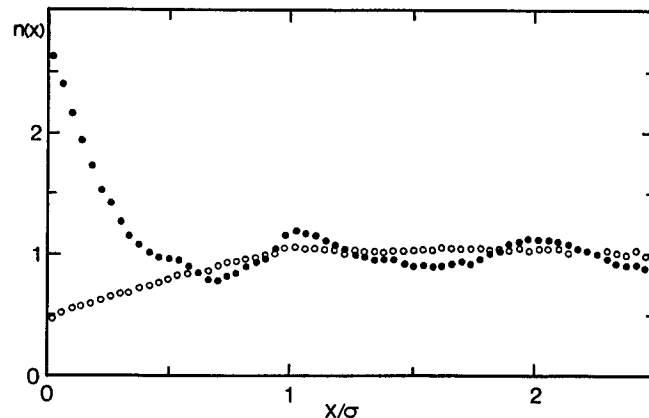


FIG. 1. Normalized segment-density profile $n(x)$ vs distance from wall, from simulations of the hard-chain fluid with $n = 4$. Open circles: bulk volume fraction $\eta_b = 0.107$; crosses: $\eta_b = 0.34$; filled circles: $\eta_b = 0.4$.

FIG. 2. Normalized segment-density profile for $n = 4$, $\eta_b = 0.417$.

higher densities, chain insertion data is of course unavailable. To test the accuracy of our results at such densities, we conducted simulations on a much larger system ($N_p = 425$, as compared with $N_p = 190$–$222$ in the previous high-density simulations). The results of the large-cell simulations, plotted as open circles in Fig. 6, are in excellent agreement with the small-cell results, Comparison between the small- and large-cell results reveals no significant finite-size effect in the compressibility, to within statistical uncertainty (about 2%). A pair of large-cell ($H = 20$ and $30$, $\eta_b = 0.1303$ and $0.0659$, respectively) simulations of 8-mers also yielded pressures which agree with the small-cell results.[25]

To rule out anisotropy, we collected orientation statistics in the large-cell studies. We determined the average bond orientation tensor



FIG. 3. Normalized segment-density profile for $n = 4$, $\eta_b = 0.437$.



FIG. 4. Normalized segment density profile for $n = 8$, $\eta_b = 0.332$ (filled circles), and $n = 16$, $\eta_b = 0.148$ (open circles).

$$B = [(n-1)N_p]^{-1}\left\langle \sum_{i=1}^{N_p}\sum_{j=1}^{n-1}\left[\mathbf{e}_i^{(j)}\,\mathbf{e}_i^{(j)} - \frac{1}{3}I\right]\right\rangle, \quad (3.1)$$

where $I$ is the unit tensor and $\langle\ \rangle$ denotes an ensemble average, in an isotropic fluid $B_{ij} = 0$. If there is a net alignment of chains with the wall, $B_{xx} < 0$; $B_{xx}$ takes its minimum value, $-1/3$, when all chains lie in the $y$–$z$ plane.

To study the effect of proximity to the wall on orientation, the cell was divided into bins (with the $i$th bin extending from $x = i - 1$ to $x = i$), into which bonded segment pairs were assigned according to their center of mass. In bins 1 and $H$, which are adjacent to the walls, $B_{xx}$ is negative, as expected. However, averages of $B_{ij}$ over the $H$-2 interior bins show that the fluid is isotropic in bulk. For example, in the $H = 22$ studies we found $B_{xx} = -0.05 \pm 0.01$ in the end
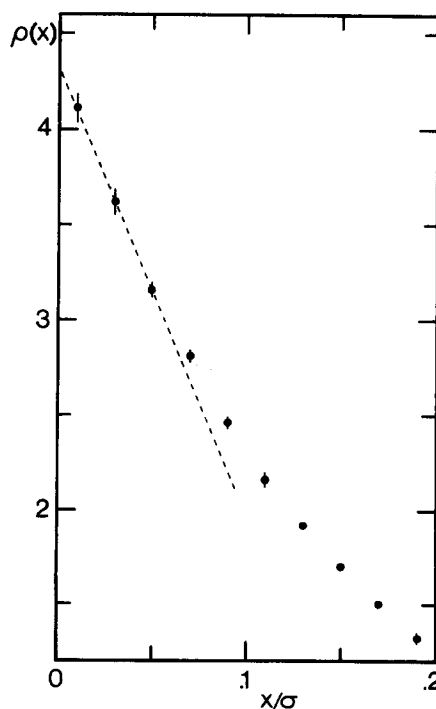


FIG. 5. Detail of the segment-density profile, $\rho(x)$, near the wall for $n = 4$, $\eta_b = 0.417$.

TABLE I. Simulation results: $n = 4$, $L = 10$.

| $N_p$ | $H$ | $\eta_{avg}$ | $\eta_b$ | $\pi^*$ | $\rho_n^{-1}\pi^*$ |
|---|---|---|---|---|---|
| 50 | 10.0 | 0.1047 | $0.1072 \pm 0.0004$ | $0.115 \pm 0.003$ | $2.25 \pm 0.06$ |
| 100 | 10.0 | 0.2094 | $0.205 \pm 0.0004$ | $0.463 \pm 0.005$ | $4.73 \pm 0.05$ |
| 130 | 10.5 | 0.2593 | $0.252 \pm 0.001$ | $0.77 \pm 0.02$ | $6.40 \pm 0.17$ |
| 130 | 10.0 | 0.2722 | $0.262 \pm 0.001$ | $0.94 \pm 0.02$ | $7.46 \pm 0.16$ |
| 134 | 9.7 | 0.2893 | $0.278 \pm 0.001$ | $1.065 \pm 0.015$ | $8.02 \pm 0.11$ |
| 140 | 9.7 | 0.3023 | $0.289 \pm 0.001$ | $1.20 \pm 0.01$ | $8.70 \pm 0.07$ |
| 160 | 10.35 | 0.3238 | $0.310 \pm 0.001$ | $1.45 \pm 0.02$ | $9.80 \pm 0.14$ |
| 160 | 9.85 | 0.3402 | $0.323 \pm 0.001$ | $1.685 \pm 0.02$ | $10.93 \pm 0.13$ |
| 160 | 9.35 | 0.3584 | $0.340 \pm 0.002$ | $1.99 \pm 0.015$ | $12.2 \pm 0.1$ |
| 160 | 8.85 | 0.3786 | $0.359 \pm 0.001$ | $2.31 \pm 0.015$ | $13.5 \pm 0.1$ |
| 190 | 9.976 | 0.3989 | $0.376 \pm 0.002$ | $2.90 \pm 0.03$ | $16.1 \pm 0.17$ |
| 190 | 9.353 | 0.4255 | $0.399 \pm 0.002$ | $3.56 \pm 0.05$ | $18.7 \pm 0.3$ |
| 190 | 8.824 | 0.4510 | $0.417 \pm 0.002$ | $4.33 \pm 0.08$ | $21.7 \pm 0.4$ |
| 222 | 10.0 | 0.4650 | $0.437 \pm 0.002$ | $5.23 \pm 0.06$ | $25.1 \pm 0.3$ |
| 425 | 25.0 | 0.3560 | $0.349 \pm 0.001$ | $2.20 \pm 0.04$ | $12.7 \pm 0.3$ |
| 425 | 22.0 | 0.4046 | $0.394 \pm 0.001$ | $3.35 \pm 0.05$ | $17.8 \pm 0.3$ |
| 425 | 21.0 | 0.4239 | $0.410 \pm 0.0015$ | $4.11 \pm 0.07$ | $21.0 \pm 0.5$ |
| 425 | 20.0 | 0.4551 | $0.4302 \pm 0.0007$ | $4.97 \pm 0.03$ | $24.2 \pm 0.2$ |

bins, and $0.005 \pm 0.01$ in the interior. The corresponding values for $H = 20$ are $-0.059 \pm 0.01$ and $0.006 \pm 0.004$. We conclude that our simulations of 4-mers (and of 8-mers, at low density), are free of significant orientational or finite-size induced errors. It is reasonable to expect the same to hold for the $n = 16$ results, which are restricted to considerably lower densities. A definitive answer must await results of large-cell simulations of 16-mers (in progress).

In Figs. 6–8 we have plotted the predictions of several theories for the hard-sphere chain system: the iterative convolution (IC) theory of Croxton,[4,5] Wertheim's theory[26] of equilibrium polymerization (W), and the generalized Flory (GF) and Flory–Huggins (GFH) theories derived in I. Each of these theories reduces to an accurate equation of state when $n = 1$ (i.e., hard spheres). In this limit, IC becomes the Percus–Yevick approximation,[27] while the other theories reduce to the Carnahan–Starling equation of state.[28] Wertheim's theory describes a polydisperse system with average chain length $n$; the other theories apply to monodisperse systems. (In Fig. 6 we have also plotted the Flory lattice formula,[9] which gives a gross underestimate of the pressure.) The comparison between theory and simulation may be summarized as follows: The IC pressure is reasonably accurate at high densities, but is much too low at low densities. The GFH prediction is quite accurate at low densities, but underestimates the pressure at high densities. GF theory, while accurate at high density, overestimates the pressure

at low densities. (This tendency is shared by the original Flory and Flory–Huggins theories, as applied to athermal lattice chains.[29]) Finally, Wertheim's theory yields an accurate pressure over the full range of densities examined in the $n = 4$ and 8 studies. For these chain lengths, Wertheim's theory is clearly the best of the four equations of state considered, notwithstanding its modest overestimate of the pressure at low and moderate densities. For $n = 16$, the presently available data seem to favor the W and GFH predictions nearly equally. Simulations of $n = 16$ (and longer) chains at higher densities should be of great value in elucidating the relative merits of the existing theories, and in guiding the development of more accurate predictions for the equation of state.

It is intuitively appealing to suppose that as $n$ becomes large, the compressibility factor per segment approaches a limit which is independent of $n$. The W, GF, and GFH theories explicitly predict that the quantity

$$Z_n^* = n^{-1}[\rho_n^{-1}\pi^*(\eta, n) - 1] \tag{3.2}$$

becomes independent of $n$ as $n \to \infty$. To test this prediction, we plot our data for $Z_n^*$, together with the limiting GF and W predictions, as a function of volume fraction in Fig. 9. An approximate scaling of the data is evident in this plot. Figures 6–9 incorporate the correction of a minor numerical error[30] in the original GF and GFH computations presented in I.

TABLE II. Simulation results: $n = 8$, $L = 10$.

| $N_p$ | $H$ | $\eta_{avg}$ | $\eta_b$ | $\pi^*$ | $\rho_n^{-1}\pi^*$ |
|---|---|---|---|---|---|
| 14 | 10.0 | 0.0586 | $0.0659 \pm 0.0004$ | $0.030 \pm 0.001$ | $1.90 \pm 0.06$ |
| 30 | 10.0 | 0.1257 | $0.1306 \pm 0.0009$ | $0.119 \pm 0.003$ | $3.79 \pm 0.08$ |
| 42 | 10.0 | 0.1759 | $0.1765 \pm 0.0002$ | $0.246 \pm 0.003$ | $5.84 \pm 0.07$ |
| 89 | 16.2 | 0.2301 | $0.227 \pm 0.001$ | $0.49 \pm 0.01$ | $9.05 \pm 0.23$ |
| 89 | 13.638 | 0.2734 | $0.267 \pm 0.001$ | $0.793 \pm 0.007$ | $12.43 \pm 0.17$ |
| 89 | 11.689 | 0.3189 | $0.308 \pm 0.002$ | $1.29 \pm 0.015$ | $17.5 \pm 0.3$ |
| 89 | 10.755 | 0.3466 | $0.332 \pm 0.0014$ | $1.74 \pm 0.02$ | $21.9 \pm 0.4$ |

TABLE III. Simulation results: $n = 16$, $L = 12$.

| $N_p$ | $H$ | $\eta_{avg}$ | $\eta_b$ | $\pi^*$ | $\rho_n^{-1}\pi^*$ |
|---|---|---|---|---|---|
| 20 | 16.0 | 0.0727 | $0.0802 \pm 0.0005$ | $0.036 \pm 0.002$ | $3.76 \pm 0.21$ |
| 34 | 13.72 | 0.1442 | $0.148 \pm 0.0013$ | $0.129 \pm 0.003$ | $7.32 \pm 0.23$ |
| 44 | 12.38 | 0.2067 | $0.2045 \pm 0.0014$ | $0.391 \pm 0.003$ | $13.2 \pm 0.4$ |
| 44 | 10.863 | 0.2356 | $0.231 \pm 0.002$ | $0.439 \pm 0.01$ | $15.9 \pm 0.3$ |
| 52 | 12.085 | 0.2503 | $0.247 \pm 0.003$ | $0.472 \pm 0.005$ | $18.2 \pm 0.3$ |
| 52 | 10.79 | 0.271 | $0.2717 \pm 0.0007$ | $0.783 \pm 0.007$ | $24.1 \pm 0.3$ |
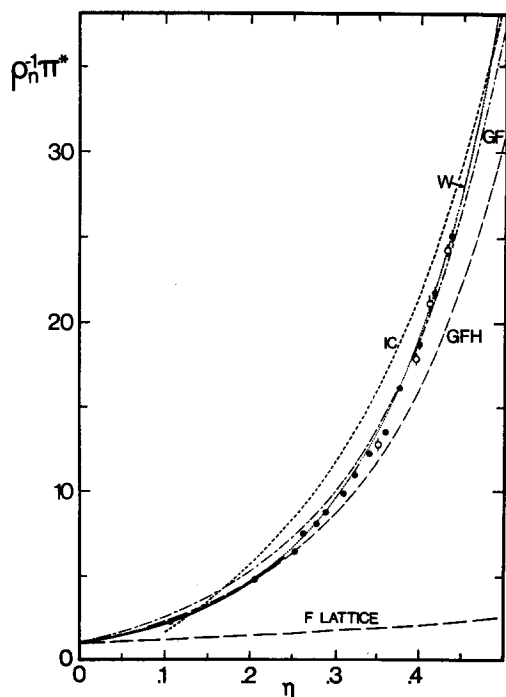


FIG. 6. Compressibility factor, $\rho_n^{-1}\pi^*$, vs bulk volume fraction $\eta_b$ for chains of $n = 4$ hard spheres. Solid line: chain-insertion Monte Carlo (I); filled circles: present simulations, $H < 10.5$; open circles: present simulations, $H > 20$. The broken lines represent various theoretical predictions as described in the text.
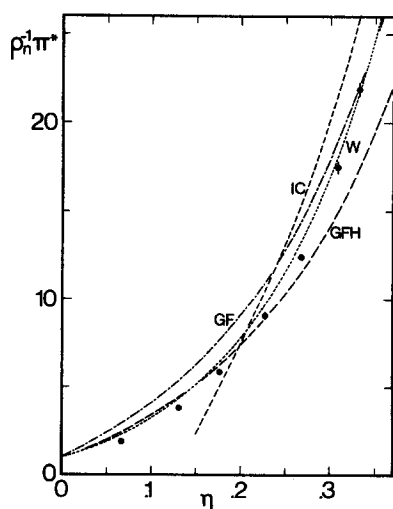


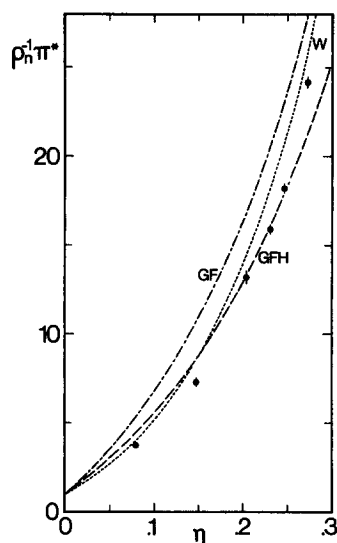FIG. 8. Compressibility factor as in Fig. 5, for $n = 16$.



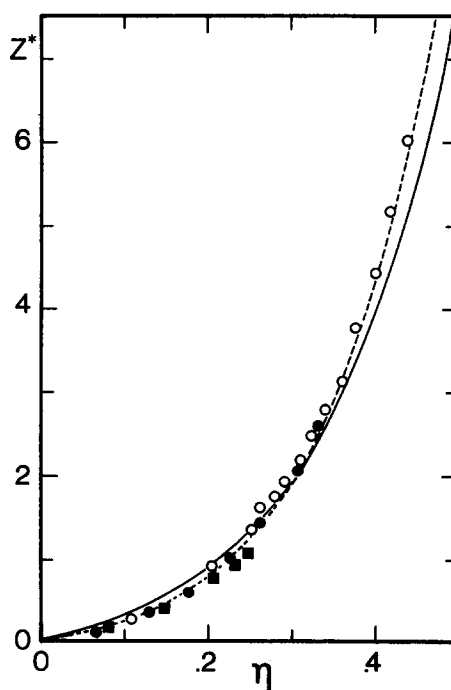FIG. 7. Compressibility factor as in Fig. 5, for $n = 8$.



FIG. 9. Test of scaling behavior of $Z_n^*$, Eq. (3.3). Open circles: $n = 4$; filled circles: $n = 8$; squares: $n = 16$. The solid and broken lines represent, respectively, the limiting ($n \to \infty$) GF and W predictions for $Z_n^*$.

In light of the results described above, it appears that accurate equations of state for fluids composed of short, flexible hard-sphere chains are now available. Their derivations make use, in one form or another, of accurate predictions for the (monomer) hard-sphere fluid, and eschew the lattice-statistics approach traditionally employed in theories of polymer solutions. It should now be feasible to derive accurate theories for the thermodynamics of chain-molecule fluids with more realistic interactions. We expect the Monte Carlo method introduced herein to prove useful in further investigations of molecular fluids.

## ACKNOWLEDGMENTS

[1] P. J. Flory, *Principles of Polymer Chemistry* (Cornell University, Ithaca, 1953).

[2] P. -G. de Gennes, *Scaling Concepts in Polymer Physics* (Cornell University, Ithaca, 1979).

[3] C. G. Gray and K. E. Gubbins, *Theory of Molecular Fluids* (Clarendon, Oxford, 1984), Vol. 1.

[4] C. A. Croxton, J. Phys. A **12**, 2497 (1979).

[5] C. A. Croxton, J. Phys. A **17**, 2129 (1984).

[6] R. Dickman and C. K. Hall, J. Chem. Phys. **85**, 4108 (1986).

[7] K. S. Schweizer and J.G. Curro, Phys. Rev. Lett. **58**, 246 (1987).

[8] J. P. Hansen and I.R. McDonald, *Theory of Simple Liquids* (Academic, New York, 1986).

[9] P. J. Flory, J. Chem. Phys. **9**, 660 (1941); M. L. Huggins, *ibid.*, **9**, 440 (1941).

[10] J. K. Percus, J. Stat. Phys. **15**, 423 (1976).

[11] B. C. Freasier, D. Jolly, and R. J. Bearman, Mol. Phys. **31**, 255 (1976); I. Aviram, D. J. Tildesley, and W. B. Streett, *ibid.* **34**, 581 (1977); I. Nezbeda and W. R. Smith, J. Chem. Phys. **75**, 4060 (1981).

[12] W. W. Wood, in *Physics of Simple Fluids*, edited by H. N. V. Temperley, G. S. Rushbrooke, and J. S. Rowlinson (North-Holland, Amsterdam, 1968), Chap. 5.

[13] I. R. McDonald, Mol. Phys. **23**, 41 (1972).

[14] J. R. Henderson and F. Van Swol, Mol. Phys. **51**, 991 (1984).

[15] N. Go and H. A. Scheraga, Macromolecules **9**, 535 (1976).

[16] M. Fixman, Proc. Natl. Acad. Sci. U.S.A. **71**, 3050 (1974).

[17] E. Helfand, J. Chem. Phys. **71**, 5000 (1979).

[18] N. Metropolis, A. W. Rosenbluth, M. N. Rosenbluth, A. H. Teller, and E. Teller, J. Chem. Phys. **21**, 1087 (1953).

[19] D. Henderson, F. F. Abraham, and J. R. Barker, Mol. Phys. **31**, 1291 (1976).

[20] E. Waisman, D. Henderson, and J. L. Lebowitz, Mol. Phys. **32**, 1373 (1976).

[21] L. Blum and G. Stell, J. Stat. Phys. **15**, 439 (1976).

[22] I. K. Snook and D. Henderson, J. Chem. Phys. **68**, 2134 (1978).

[23] L. J. Lowden and D. Chandler, J. Chem. Phys. **59**, 6587 (1973); B. M. Ladanyi and D. Chandler, *ibid.* **62**, 4308 (1975); C. S. Hsu, L. R. Pratt, and D. Chandler, *ibid.* **68**, 4213 (1978).

[24] W. B. Streett and D. J. Tildesley, J. Chem. Phys. **68**, 1275 (1978); J. Talbot and D. J. Tildesley, *ibid.* **83**, 6419 (1985).

[25] K. Honnell (personal communication).

[26] M. S. Wertheim, J. Chem. Phys. **87**, 7323 (1987).

[27] J. K. Percus and G. J. Yevick, Phys Rev. **110**, 1 (1958); E. Thiele, J. Chem. Phys. **39**, 474 (1963); M. S. Wertheim, Phys. Rev. Lett. **10**, 321 (1963); J. Math. Phys. **5**, 643 (1964).

[28] N. F. Carnahan and K. E. Starling, J. Chem. Phys. **51**, 635 (1969).

[29] R. Dickman and C. K. Hall, J. Chem. Phys. **85**, 3023 (1986).

[30] The values for the triple-overlap integrals quoted in I are incorrect. The correct value for the 3D integral [Eq. (A.5) of I] is $0.374\,95\sigma^3$. The trimer exclusion volume, Eq. (A.6), then becomes $v_e(3) = 2v_e(2) - v_e(1) - 0.122\,33\sigma^3 = 9.826\,05\sigma^3$. The net effect of this correction is to raise the GF and GFH predictions for the pressure by about 1.9%. For hard disks, the correct value for $v_e(3)$ is $6.88\,159\sigma^2$. We are grateful to Kevin Honnell for bringing this error to our attention.